Conformational Relaxation following Hydride Transfer Plays a Limiting Role in Dihydrofolate Reductase Catalysis[†]

David D. Boehr, H. Jane Dyson, and Peter E. Wright*

Department of Molecular Biology and Skaggs Institute for Chemical Biology, The Scripps Research Institute, 10550 North Torrey Pines Road, La Jolla, California 92037

Received June 11, 2008; Revised Manuscript Received July 15, 2008

ABSTRACT: The catalytic cycle of an enzyme is frequently associated with conformational changes that may limit maximum catalytic throughput. In *Escherichia coli* dihydrofolate reductase, release of the tetrahydrofolate (THF) product is the rate-determining step under physiological conditions and is associated with an "occluded" to "closed" conformational change. In this study, we demonstrate that in dihydrofolate reductase the closed to occluded conformational change in the product ternary complex (E·THF·$NADP^+$) also gates progression through the catalytic cycle. Using NMR relaxation dispersion, we have measured the temperature and pH dependence of microsecond to millisecond time scale backbone dynamics of the occluded E·THF·$NADP^+$ complex. Our studies indicate the presence of three independent dynamic regions, associated with the active-site loops, the cofactor binding cleft, and the C-terminus and an adjacent loop, which fluctuate into discrete conformational substates with different kinetic and thermodynamic parameters. The dynamics of the C-terminally associated region is pH-dependent ($pK_a < 6$), but the dynamics of the active-site loops and cofactor binding cleft are pH-independent. The active-site loop dynamics access a closed conformation, and the accompanying closed to occluded rate constant is comparable to the maximum pH-independent hydride transfer rate constant. Together, these results strongly suggest that the closed to occluded conformational transition in the product ternary complex is a prerequisite for progression through the catalytic cycle and that the rate of this process places an effective limit on the maximum rate of the hydride transfer step.

Many enzymes have evolved to the point where chemical bond-breaking and bond-making events are no longer rate-limiting (*1*). Instead, conformational changes required to bind substrate, orient the reactants, or release products may limit catalytic turnover (*2*). A comprehensive understanding of the limits on enzyme catalytic rates thus requires an understanding of both the chemical events at the active site and the physical processes that are required for catalytic turnover. Both considerations are important in de novo enzyme engineering and drug design efforts.

Escherichia coli dihydrofolate reductase (DHFR)[1] is an excellent model system for understanding the role of protein dynamics in enzymatic catalysis. DHFR catalyzes the reduction of 7,8-dihydrofolate (DHF) through stereospecific hydride transfer from the reduced nicotinamide adenine dinucleotide phosphate (NADPH) cofactor (*3, 4*). The enzyme is both an anticancer and antimicrobial drug target and has been the subject of extensive structural (*5*), functional (*6*), and theoretical studies (*7*). Analysis of pre-steady-state kinetics has demonstrated that *E. coli* DHFR cycles through five major states under physiological conditions (*8*): the holoenzyme (E·NADPH), the Michaelis complex (E·DHF·NADPH), and three tetrahydrofolate product complexes [the product ternary complex (E·THF·$NADP^+$) formed immediately following hydride transfer, the product binary complex (E·THF) formed by dissociation of the oxidized cofactor, and the product release complex (E·THF·NADPH)]. At physiological pH, the rate-limiting step is the release of THF product from the E·THF·NADPH complex.

DHFR is a relatively small protein (159 residues) comprised of a mixed eight-strand β-sheet flanked by four α-helices and several flexible loops. Extensive structural characterization of the enzyme revealed three major conformations in the crystalline state (*5*), although only the "closed" and "occluded" conformations have been observed under solution conditions (*9*). The closed and occluded conformations differ in the structure of the active-site Met20 loop. The closed conformation, observed in the holoenzyme (E·NADPH) and the Michaelis model complexes (E·FOL·$NADP^+$ and E·DHF·$NADP^+$) (*9*), is stabilized through hydrogen bonding interactions between the Met20 and FG loops (*5*). Following hydride transfer, the product ternary complex E·THF·$NADP^+$ assumes an occluded ground-state structure (Figure 1). The hydrogen bonds between the Met20 and FG loops break, and new hydrogen bonds are formed between the Met20 and GH loops to

[†] This work was supported by Grant GM75995 from the National Institutes of Health. D.D.B. was the recipient of a Canadian Institutes of Health Research postdoctoral fellowship.

* To whom correspondence should be addressed. E-mail: wright@scripps.edu. Telephone: (858) 784-9721. Fax: (858) 784-9822.

[1] Abbreviations: DHFR, dihydrofolate reductase; FOL, folic acid; DHF, dihydrofolate; THF, tetrahydrofolate; NADPH, nicotinamide adenine dinucleotide phosphate, reduced form; $NADP^+$, nicotinamide adenine dinucleotide phosphate, oxidized form; CPMG, Carr−Purcell−Meiboom−Gill; NMR, nuclear magnetic resonance; HSQC, heteronuclear single-quantum correlation; HMQC, heteronuclear multiple-quantum correlation.

10.1021/bi801102e CCC: $40.75
Published on Web 08/09/2008

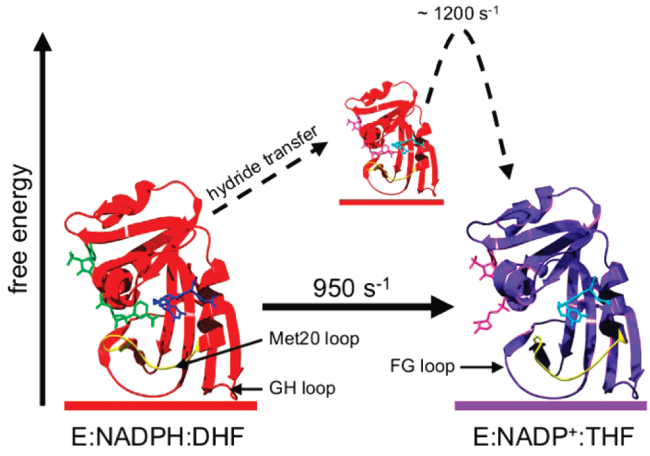

FIGURE 1: Conformational dynamics in *E. coli* dihydrofolate reductase govern catalytic turnover. Prior to hydride transfer, the Met20 loop is in a closed conformation (left, PDB entry 1RX2) but adopts an occluded conformation following hydride transfer (right, PDB entry 1RX4). The rate constant for the closed to occluded transition in E·THF·$NADP^+$ determined by R_2 relaxation dispersion (*21*) is strikingly similar to the maximum pH-independent hydride transfer rate constant (*8*). NADPH, DHF, $NADP^+$, and THF are colored green, blue, pink, and cyan, respectively. The Met20 loop is highlighted in yellow.

stabilize the occluded conformation. In the occluded conformation, the nicotinamide ring of the cofactor is sterically hindered from entering the active site, and thus, chemistry can occur only through a closed conformation. The occluded conformation is observed in the three product complexes of wild-type DHFR: E·THF·$NADP^+$, E·THF, and E·THF·NADPH (*9*). The cycling between closed and occluded conformations is critical for progress around the enzymatic cycle. Mutations that disrupt either the closed or occluded conformations lead to decreases in the rate of hydride transfer and/or steady-state catalytic turnover (*10*−*15*).

We have used nuclear magnetic resonance (NMR) to study the dynamic properties of *E. coli* DHFR as it traverses its catalytic cycle (*16*−*21*). In particular, we have used R_2 relaxation dispersion spectroscopy to analyze the microsecond to millisecond time scale dynamics of DHFR at each step of the catalytic cycle (*20, 21*). R_2 relaxation dispersion is a measure of how well conformational exchange contributions (R_{ex}) to the transverse relaxation rate constant (R_2) can be suppressed by the 180° refocusing pulses in a Carr−Purcell−Meiboom−Gill (CPMG) pulse train (*22, 23*). For two-site exchange between a lower-energy conformation (A) and a higher-energy conformation (B), analysis of relaxation dispersion curves provides information about the kinetics of the conformational exchange between A and B ($k_{ex} = k_{AB} + k_{BA}$), the populations of states A and B (p_A and p_B, respectively), and the chemical shift difference ($\Delta\omega$) between sites A and B (*24*).

For *E. coli* DHFR, R_2 relaxation dispersion experiments have shown that at each step of the catalytic cycle, the enzyme adopts a major substate represented by the X-ray structure of that intermediate (or of complexes that model the intermediate), and one or more minor substates that are structurally similar to either the next or prior intermediate in the catalytic cycle (*21*). In particular, the product ternary complex E·THF·$NADP^+$ has an occluded major substate and a closed minor substate that is structurally similar to the Michaelis model complex E·FOL·$NADP^+$. Moreover, the rate constant determined from R_2 relaxation dispersion ($k \sim 1200\ s^{-1}$) for the conversion of the higher-energy closed substate to the lower-energy occluded substate of E·THF·$NADP^+$ is very similar to the maximum pH-independent hydride transfer rate constant ($950\ s^{-1}$) for conversion from substrate to product, suggesting that the pH-independent rate constant may be limited by the closed to occluded conformational change in E·THF·$NADP^+$. In addition, dynamic processes were observed in the cofactor binding site due to fluctuations involving a minor substate that is similar in structure to the E·THF complex (*21*).

In this study, we have further explored the energy landscape of the E·THF·$NADP^+$ complex by measuring microsecond to millisecond protein dynamics under a more extensive array of temperature and pH conditions. Our experiments reveal three separate dynamic events in the protein and indicate that physical changes within the energy landscape of the product ternary complex are tightly linked to maximum rates of hydride transfer.

MATERIALS AND METHODS

Protein Purification and Sample Preparation. E. coli DHFR was expressed and purified according to previously established procedures (*21*). The ligands $NADP^+$ and THF are light and/or oxygen sensitive and must be treated accordingly. Before sample preparation, buffer was thoroughly degassed through freeze−pump−thaw cycles using a vacuum apparatus, and ascorbic acid was added to act as an oxygen scavenger. The final samples contained 1 mM DHFR, 10 mM $NADP^+$, 6 mM THF, 1 mM DTT, 25 mM KCl, and 10% D_2O in 70 mM KP_i (pH 6.1−7.6). The samples were placed in amberized NMR tubes, subjected to vacuum again, overlaid with argon, and flame-sealed to prevent buffer reoxidization. Under these conditions, the samples are stable for R_2 relaxation dispersion measurements for ~1 week.

R_2 Relaxation Dispersion Experiments. ^{15}N R_2 relaxation rates were measured at ^1H spectrometer frequencies of 500 and 800 MHz using relaxation-compensated CPMG pulse sequences in a constant-time manner as previously described (*20, 22*). The total relaxation time was 40 ms. The R_2 relaxation dispersion data were fit simultaneously at the two frequencies using the in-house computer program GLOVE with the following series of equations describing conformational exchange between two sites, A and B:

$$R_2(1/\tau_{CP}) = R_2^0 + \frac{1}{2}\left\{k_{ex} - \frac{1}{\tau_{CP}}\cosh^{-1}[D_+\cosh(\eta_+) - D_-\cos(\eta_-)]\right\} \quad (1)$$

in which

$$D_\pm = \frac{1}{2}\left[\pm 1 + \frac{\psi + 2\Delta\omega^2}{(\psi^2 + \zeta^2)^{1/2}}\right]^{1/2} \quad (2)$$

$$\eta_\pm = \frac{\tau_{CP}}{2}[\pm\psi + (\psi^2 + \zeta^2)^{1/2}]^{1/2} \quad (3)$$

where $\psi = k_{ex}^2 - \Delta\omega^2$, $\zeta = -2\Delta\omega k_{ex}(p_A - p_B)$, τ_{cp} is the time between successive 180° pulses in the CPMG pulse train, R_2^0 is the R_2 relaxation rate in the absence of conformational exchange, p_A and p_B are the populations of

Table 1: Kinetic and Thermodynamic Fitting Parameters for Wild-type E·THF·NADP$^+$ ^{15}N R_2 Relaxation Dispersion Curves at Different pHs and Temperatures

	cluster 1, active-site loops		cluster 2, cofactor binding cleft		cluster 3, C-terminal associated region	
	k_{ex} (s^{-1})	$p_A p_B$	k_{ex} (s^{-1})	$p_A p_B$	k_{ex} (s^{-1})	$p_A p_B$
pH 7.6						
294 K	985 ± 23	0.008 ± 0.000	nd[a]	nd[a]	529 ± 142	0.013 ± 0.001
297 K	1210 ± 55	0.010 ± 0.000	600 ± 118	0.019 ± 0.011	586 ± 50	0.015 ± 0.001
300 K	1300 ± 47	0.014 ± 0.000	1700 ± 116	0.029 ± 0.017	550 ± 30	0.022 ± 0.001
303 K	1624 ± 76	0.017 ± 0.001	nd[a]	nd[a]	666 ± 42	0.028 ± 0.001
306 K	1832 ± 129	0.019 ± 0.002	nd[a]	nd[a]	700 ± 54	0.033 ± 0.001
pH 7.0						
297 K	1352 ± 73	0.010 ± 0.001	598 ± 73	0.040 ± 0.015	532 ± 20	0.021 ± 0.001
300 K	1470 ± 70	0.014 ± 0.001	1739 ± 53	0.028 ± 0.009	588 ± 15	0.025 ± 0.001
pH 6.5						
294 K	913 ± 92	0.008 ± 0.000	nd[a]	nd[a]	662 ± 85	0.019 ± 0.002
297 K	1280 ± 41	0.010 ± 0.001	558 ± 61	0.032 ± 0.006	521 ± 25	0.024 ± 0.001
300 K	1350 ± 44	0.014 ± 0.001	1726 ± 212	0.028 ± 0.005	523 ± 19	0.028 ± 0.009
303 K	1652 ± 488	0.016 ± 0.009	nd[a]	nd[a]	550 ± 65	0.031 ± 0.002
pH 6.1						
294 K	949 ± 68	0.008 ± 0.000	nd[a]	nd[a]	419 ± 61	0.018 ± 0.002
300 K	1500 ± 200	0.014 ± 0.001	1400 ± 320	0.025 ± 0.003	463 ± 40	0.032 ± 0.002
303 K	1640 ± 108	0.018 ± 0.003	nd[a]	nd[a]	450 ± 40	0.038 ± 0.002

[a] Not determined; although conformational exchange is still apparent in the cofactor binding cleft, the R_2 relaxation dispersion curves are not of sufficient quality to determine $\Delta\omega$, k_{ex}, or $p_A p_B$ values.

the ground- and excited-state conformations, respectively ($p_A + p_B = 1$), and $\Delta\omega$ is the chemical shift difference between substates A and B. Rate constants for the transitions from the ground state to excited state (k_{AB}) and from the excited state to ground state (k_{BA}) can be determined by $p_B k_{ex}$ and $p_A k_{ex}$ respectively. Residues generally fit into one of three clusters, including the active-site loops and other residues around the active site, cofactor binding site, or the C-terminal associated region. Each cluster was fit with global k_{ex} and $p_A p_B$ values while allowing $\Delta\omega$ values to vary for each residue. The clusters showed significantly different k_{ex} and $p_A p_B$ values (Table 1). In Table S1 of the Supporting Information, we report $\Delta\omega$ values following global fitting procedures. However, in a few select cases, $\chi^2_{global}/\chi^2_{individual} > 2$, so we report only the $\Delta\omega$ value for the individual fit.

pH and Temperature Dependence of Protein Dynamics. R_2 relaxation dispersion measurements were performed using four different pH conditions (pH 6.1, 6.5, 7.0, and 7.6) and up to five different temperatures (294, 297, 300, 303, and 306 K) (Table 1). Only the dynamics in the C-terminal associated region showed a dependence on pH.

The enthalpy (ΔH) and entropy ($-T\Delta S$) energy differences between the excited- and ground-state conformations can be estimated through the temperature dependence of the conformational exchange equilibrium constant using van't Hoff analysis according to eq 4

$$\ln K = -\Delta H/RT + \Delta S/R \quad (4)$$

where K is equal to k_{BA}/k_{AB}. Reported errors are based on jackknife simulations (*20, 21*). The activation barriers can be estimated using transition-state theory, according to eq 5

$$k = (k_B T/h)e^{\Delta S^{\ddagger}/R}e^{-\Delta H^{\ddagger}/RT} \quad (5)$$

where k is the rate constant measured from R_2 relaxation dispersion (k_{AB}), k_B is Boltzmann's constant, h is Planck's constant, R is the universal gas constant, T is the temperature, $\Delta S^{\ddagger}$ is the entropy of activation, and $\Delta H^{\ddagger}$ is the enthalpy of activation.

An alternative to transition-state theory is the phenomenological Ferry law (*25, 26*) that describes a lower energy barrier with a rough enthalpic surface according to eq 6

$$\ln k = \ln C - [\Delta H_0^{\ddagger}/RT + \langle H^2\rangle^{1/2}/(RT)^2] \quad (6)$$

where k is the rate constant measured from R_2 relaxation dispersion (k_{AB}), C is a constant, R is the universal gas constant, T is the temperature, $\Delta H_0^{\ddagger}$ is the enthalpy of activation associated with the smooth Arrhenius-like barrier height, and $\langle H^2\rangle^{1/2}$ is the enthalpy due to the ruggedness of the barrier.

RESULTS

Relaxation Dispersion in the E·THF·NADP$^+$ Complex. Relaxation dispersion curves were measured under a wide range of conditions using relaxation-compensated CPMG pulse sequences (*22*), as described in Materials and Methods. These data extend previous measurements performed at pH 7.6 and 300 K (*21*). Residues with conformational exchange were mapped to three regions: the active-site loops (Met20, FG, and GH loops), the cofactor binding cleft, and the C-terminal associated region (residues 129−134 and 155−159) (Figure 2A). The kinetics and thermodynamics of the protein conformational fluctuations differ significantly among the three clusters. The k_{ex} (p_B) values are 1300 ± 50 s^{-1} (1.4%), 1700 ± 120 s^{-1} (2.9%), and 550 ± 30 s^{-1} (2.2%) at pH 7.6 and 300 K for the active-site loops, cofactor binding cleft, and C-terminal associated region, respectively (Table 1). Since k_{ex} and p_B values for each cluster are substantially different across several pH and temperature conditions (Table 1), we conclude that that the E·THF·NADP$^+$ complex populates at least three independent higher-energy substates as a result of conformational fluctuations.

pH Dependence of the Dynamic Events in the E·THF·NADP$^+$ Complex. To gain further insight into the apparent correlation between the maximum hydride transfer rate and the rate of the conformational relaxation from the closed excited state to the occluded ground state of the E·THF·NADP$^+$ complex, ^{15}N R_2 relaxation dispersion

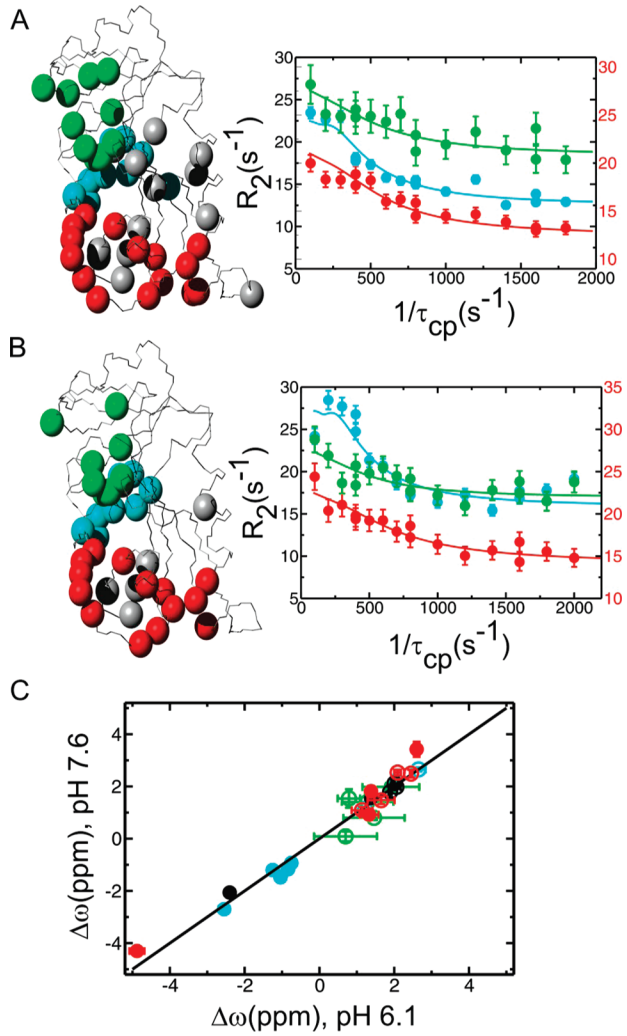

FIGURE 2: Conformational exchange as measured by R_2 relaxation dispersion in the product ternary E·THF·NADP$^+$ complex of DHFR at pH 7.6 (A) and 6.1 (B). (A and B) Residues displaying conformational exchange (R_{ex}) are highlighted as colored spheres on the E·THF·NADP$^+$ structure (PDB entry 1RX4) according to the cluster to which they belong (red and gray for active-site loops and associated residues, green for the cofactor binding cleft, and blue for the C-terminal associated region). Representative R_2 relaxation dispersion curves from each dynamic cluster are shown on the right (red for Gly121, green for Thr46, and blue for Asp131). Data were collected at two external magnetic fields (^{1}H, 500 and 800 MHz), but only 800 MHz field data are shown here for clarity. R_2 rate constants for the red Gly121 curves are plotted on the right-hand *y*-axis to improve clarity. (C) Higher-energy substates observed at pH 6.1 and 7.6 are similar as indicated by the 1:1 linear correlation between the dynamic chemical shift differences ($\Delta\omega$) observed in the R_2 relaxation dispersion experiments under the two pH conditions. Data points are color-coded as described above. Filled circles indicate that the sign of $\Delta\omega$ could be determined for both pHs using an HMQC/HSQC comparison according to ref *51*. Empty circles indicate that the sign could not be determined for one or both pH conditions.

measurements were made for the E·THF·NADP$^+$ complex under varying pH conditions (pH 6.1−7.6). The dynamic events at the active-site loops and in the cofactor binding cleft are not dependent on pH. Similar residues showed dispersive behavior throughout the pH range (Figure 2B), and $\Delta\omega$ values are nearly identical at each pH (Figure 2C and Table S1 of the Supporting Information), suggesting that the identity of the higher-energy substates corresponding to these dynamic events does not change significantly with pH.

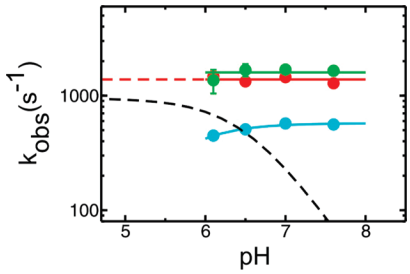

FIGURE 3: pH dependence of the conformational exchange kinetics in the E·THF·NADP$^+$ complex at 300 K. The rate constants for the transition from the excited state to the ground state (k_{BA}) for the active-site loops, cofactor binding cleft, and C-terminal associated region are plotted in red, green, and blue, respectively. The dashed black curve is a simulation of the pH dependence of the hydride transfer rate constant with a pK_a of 6.5 and pH-independent rate constant of 950 s^{-1} (at 298 K) (*8*).

The kinetic (k_{ex}) and thermodynamic (p_B) parameters for these dynamic events also remained relatively constant from pH 6.1 to 7.6 (Figure 3), and a change in temperature resulted in identical changes to these parameters under all pH conditions (Table 1).

In contrast, the dynamic process in the C-terminal associated region of DHFR was observed to be pH-dependent with a pK_a of <6 (Figure 3). As the pH decreased from 7.6 to 6.1, k_{ex} decreased and *p*B increased, but the $\Delta\omega$ values remained identical (Table S1 of the Supporting Information). This suggested that although the kinetics and thermodynamics of the dynamic process in the C-terminal region change with pH, the higher-energy substate remains identical throughout the pH range of the experiments.

Temperature Dependence of the Dynamic Events in the E·THF·NADP$^+$ Complex. Measurements of R_2 relaxation dispersion as a function of temperature can provide further insight into the conformational energy surface in terms of entropy and enthalpy contributions. The population (p_B) of the higher-energy substate associated with the dynamic event at the active-site loops increases with temperature (Figure 4A). A van't Hoff-type analysis of this trend indicates that the higher-energy closed substate is enthalpically disfavored ($\Delta H = 13.9 \pm 0.5$ kcal/mol), but it is entropically favored ($-T\Delta S = -11.2 \pm 0.5$ kcal/mol at 298 K) over the occluded ground-state structure [ΔG(closed−occluded) $= 2.7 \pm 0.5$ kcal/mol at 298 K]. Again, it should be noted that $\Delta\omega$ values do not significantly change with temperature (Table S1 of the Supporting Information), indicating that the identity of the higher-energy substate remains the same over the entire pH and temperature range.

For the C-terminal associated residues, the higher-energy substate is also enthalpically disfavored ($\Delta H = 15.5 \pm 0.5$ kcal/mol) and entropically favored ($-T\Delta S = -13.1 \pm 0.5$ kcal/mol; $\Delta G = 2.4 \pm 0.5$ kcal/mol at 298 K) (Figure 4B). However, these values are significantly different from the values for the closed to occluded conformational change, again indicating the dynamic processes in the active-site loops and the C-terminal associated region are largely independent.

We have previously estimated the activation barrier associated with the occluded to closed conformational change in the E·FOL·NADP$^+$ complex using transition-state theory (*20*). For E·FOL·NADP$^+$, the calculated energy barrier has a $\Delta G^‡$ of 16.0 kcal/mol, a $\Delta H^‡$ of 21.2 kcal/mol, and a

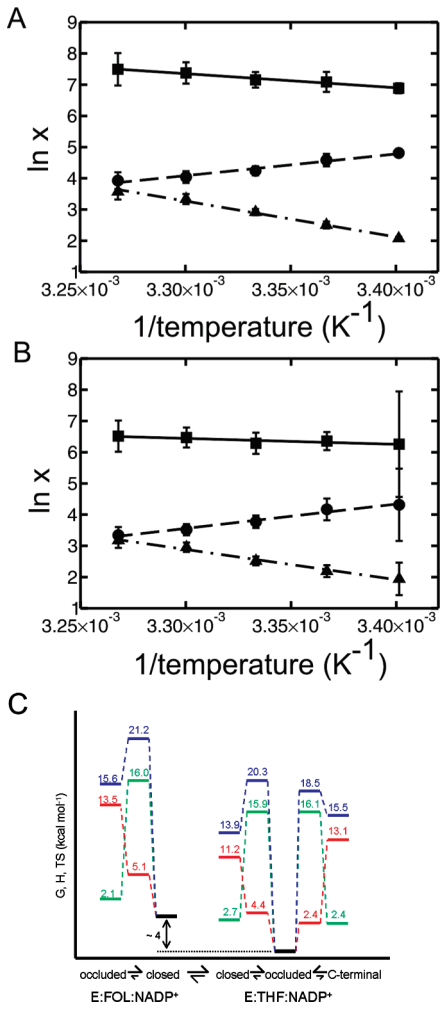

FIGURE 4: Temperature dependence of the conformational exchange kinetics in the E·THF·NADP$^+$ complex at pH 7.6 for the (A) active-site loops and (B) C-terminal associated region. Rate constants for the transitions from the excited state to the ground state [k_{BA} (■)] and from the ground state to the excited state [k_{AB} (▲)] and the equilibrium constant [k_{BA}/k_{AB} (●)] are plotted. (C) Thermodynamic comparison of E·FOL·NADP$^+$ and E·THF·NADP$^+$ complexes at 298 K. Thermodynamic barriers were calculated using transition-state theory as described in Materials and Methods. Green, blue, and red traces represent ΔG, ΔH, and $T\Delta S$, respectively. E·FOL·NADP$^+$ is a model for the E·DHF·NADPH Michaelis complex.

$-T\Delta S^{\ddagger}$ of −5.1 kcal/mol at 298 K (*20*). In a similar manner, we calculated energy barriers for protein dynamics in the active-site loops ($\Delta G^{\ddagger} = 15.9 \pm 0.5$ kcal/mol, $\Delta H^{\ddagger} = 20.3 \pm 0.5$ kcal/mol, and $-T\Delta S^{\ddagger} = -4.4 \pm 0.5$ kcal/mol) and the C-terminal associated region ($\Delta G^{\ddagger} = 16.1 \pm 0.4$ kcal/mol, $\Delta H^{\ddagger} = 18.5 \pm 0.4$ kcal/mol, and $-T\Delta S^{\ddagger} = -2.4$ kcal/mol) for E·THF·NADP$^+$ at 298 K (Figure 4C). However, it should be noted that these values represent upper limits to the true activation parameters, considering the limitations of transition-state theory in describing multidimensional, diffusive events such as protein folding and conformational change (*27, 28*).

An alternative to transition-state theory is the phenomenological Ferry law (*25, 26*) that incorporates a lower energy barrier with a rough enthalpic surface. While the accessible temperature range is too small to allow meaningful fits to this model, we estimate the enthalpy due to the ruggedness of the landscape ($\langle H^2 \rangle^{1/2}$) to be in the range of 1.8−2.6 kcal/mol for both the active-site loop and C-terminal associated regions, assuming that the activation enthalpy associated with the smooth (Arrhenius-like) part of the barrier $\Delta H_0^{\ddagger} = 0-10$ kcal/mol. The estimated values of $\langle H^2 \rangle^{1/2}$ are in agreement with the ruggedness of the enthalpic barriers for collective protein motions involving multiple atoms and interactions determined for other systems (*26, 29*).

DISCUSSION

In recent years, there has been renewed discussion about the role played by protein dynamics in enzyme catalysis (*4, 30*). Enzymes must bind diverse ligands as they traverse their catalytic cycles, and thus, they undergo a variety of conformational changes as they bind substrate(s), catalyze the chemical step(s), and release products (*2*). At any stage of the catalytic cycle, these conformational changes may become rate-limiting. Recent results from NMR studies of protein dynamics in *E. coli* DHFR and other enzymes (*20, 21, 31*−*34*) suggest that limits to catalytic rates in enzymes are intimately related to conformational exchange rates measured by R_2 relaxation dispersion. Although much progress has been made in small molecule and antibody catalysis, design efforts have failed to achieve the remarkable specificity and catalytic power of naturally occurring enzymes. This may be in part due to our inability to recapitulate the intricate orchestration of conformational changes involved in biocatalysis.

E. coli DHFR has served as a model system for the study of the interplay between protein dynamics and enzyme function (*3*). NMR, computer simulations, and single-molecule studies have all indicated the importance of protein dynamics in the catalytic cycle of DHFR. For example, computer simulations have identified a "correlated network of coupled motion" that acts to decrease the donor−acceptor distance for very efficient hydride transfer (*35*). Site-directed mutagenesis of residues within the network has confirmed their importance (*35*−*37*), and kinetic isotope effect (KIE) (*38*−*40*) and single-molecule studies (*41*−*43*) of the WT and mutant-catalyzed reaction have further underscored the essential role of protein dynamics in gating the distance between hydride donor and acceptor atoms for catalytic function. Similar results have been found for other enzymes that catalyze hydrogen transfer, including alcohol dehydrogenase (*44, 45*) and soybean lipoxygenase (*46*).

Outside of the catalytic step itself, protein dynamics play a critical role in binding substrates to and releasing products from DHFR. At physiological pH, the rate-limiting step is release of THF product from the product release complex E·THF·NADPH (12.5 s^{-1}) (*8*). We have previously shown through R_2 relaxation dispersion techniques that E·THF·NADPH accesses a higher-energy substate structurally similar to E·NADPH with a rate constant of 13−18 s^{-1} (*21*). These results argue strongly that product release occurs through the higher-energy substate, and thus, steady-state turnover is rate-limited by the conversion of the ground state to the excited substate (k_{AB}) in E·THF·NADPH.

Similarly, we have noted that the rate constant for the conversion from the excited substate to the ground state (k_{BA}) in E·THF·NADP$^+$ is strikingly similar to the pH-independent maximum hydride transfer rate constant (*21*). Many of the residues that significantly change the ^{15}N chemical shift

between the closed and occluded conformations of DHFR exhibit ^{15}N R_2 relaxation dispersion, and moreover, the dynamic chemical shifts ($\Delta\omega$) for these residues correspond to the ground-state chemical shift differences ($\Delta\delta$) between closed and occluded conformations. These results indicate that the E·THF·NADP$^+$ complex fluctuates between an occluded ground state and a higher-energy closed substate. This work adds significant new insights by showing that the rate of the closed to occluded transition in E·THF·NADP$^+$ is pH-independent. Taken together, these and the previous results suggest that the rate at which the closed excited state formed immediately following hydride transfer relaxes to the occluded ground state of the E·THF·NADP$^+$ product complex also places an effective limit on maximum enzymatic turnover. In effect, once hydride donor and acceptor atoms are properly positioned within the active site, hydride transfer is instantaneous (or at least $k_{hydride} \gg 950$ s^{-1}) (*4*), but the closed E·THF·NADP$^+$ complex must still collapse into the ground-state occluded conformation before continuing through the catalytic cycle. It should be emphasized that the closed excited state measured using R_2 relaxation dispersion does not result from back hydride transfer. The hydride transfer reaction is strongly pH-dependent (*8*); on the other hand, k_{ex} for the closed to occluded conformational change is pH-independent, and the back reaction is very much slower (0.03 s^{-1}) near neutral pH than the rate of formation of the closed excited state ($k_{AB} = 20$ s^{-1}).

Other regions within the E·THF·NADP$^+$ complex also exhibit significant conformational exchange, including the cofactor binding cleft and the C-terminal associated region. We have previously shown that the cofactor binding cleft accesses a conformation similar in structure to that found in E·THF, that is, a conformation without cofactor bound (*21*). The C-terminal associated region (residues 129−134 and 155−159), unlike the cofactor binding cleft and active-site loops, shows dispersive behavior in every complex of DHFR so far studied. Although we do not have a relevant structural model for this dynamic event, it should be noted that the dynamic chemical shifts ($\Delta\omega$) are similar for all complexes in the catalytic cycle. In this context, these motions can be seen as "intrinsic dynamics" (*33*) of the enzyme, although the role of these motions, if any, is unknown. It is noteworthy that the kinetic (k_{ex}) and thermodynamic (p_B) parameters for this dynamic event change depending on the ligand-bound state of the enzyme. For example, in the E·FOL·NADP$^+$ complex, k_{ex} is much higher (1010 s^{-1} at pH 6.8 and 303 K) (*20*) than in the E·THF·NADP$^+$ complex ($k_{ex} = 550$ s^{-1} at pH 6.5 and 303 K). This is in contrast to the dynamics at the active-site loops where k_{ex} in E·FOL·NADP$^+$ is much lower (477 s^{-1} at pH 6.8 and 303 K) than that seen for E·THF·NADP$^+$ (1650 s^{-1} at pH 6.5 and 303 K). These differences may be related to the overall conformation of the enzyme (closed vs occluded) and/or the occupancy of the substrate/product binding pocket. The change from faster to slower C-terminal dynamics between E·FOL·NADP$^+$ and E·THF·NADP$^+$ may be important in the overall configuration energy of the enzyme and may compensate for the change in dynamics observed in the active-site loops.

The motions of the three dynamic regions in the E·THF·NADP$^+$ complex are independent. The three clusters yield different global k_{ex} and p_B values and exhibit different pH and temperature dependence. Although the dynamics of the active-site loops and the cofactor binding cleft are pH-independent, the dynamics of the C-terminal associated region are clearly pH-dependent with a pK_a of <6. The C-terminal and active-site loop motion can also be differentiated on the basis of temperature dependence and, hence, on enthalpy and entropy contributions to the overall Gibbs free energy. Thus, independent dynamic events can be differentiated on the basis of their response to pH, temperature, mutagenesis, and other solvent effects [e.g., solvent isotope effect (*47, 48*)], and these approaches can be used to further characterize protein motions in larger and more complex enzyme systems where multiple dynamics events are likely.

Enzymes are inherently dynamic, and changes in conformation are required for efficient substrate binding and product release. In this study, we have demonstrated that, in DHFR, the closed to occluded conformational change associated with relaxation of the product ternary complex into its ground state following chemical reaction occurs at a rate very similar to that of maximum hydride transfer. This may not be surprising if we consider that under physiological conditions, the rate-limiting step is not chemistry, but release of THF from the enzyme. Within this evolutionary context, hydride transfer needs only to be optimized to the same extent as the release of product from the E·THF·NADPH complex and the accompanying occluded to closed conformational change, which in turn must be related back to the reverse closed to occluded conformational change in E·THF·NADP$^+$ and hydride transfer. In this manner, the kinetics and thermodynamics of the closed to occluded transition (i.e., physical changes within the energy landscape of DHFR) intimately link, and ultimately dictate, both steady-state turnover and maximum hydride transfer. These findings are entirely consistent with the dynamic energy landscape view of enzyme catalysis (*21, 49, 50*)

ACKNOWLEDGMENT

We thank John Chung and Gerard Kroon for helping with the NMR experiments and Euvel Manapalaz and Linda Tennant for excellent technical expertise.

SUPPORTING INFORMATION AVAILABLE

A table containing dynamic chemical shift information from ^{15}N R_2 relaxation dispersion experiments and figures detailing full R_2 relaxation dispersion results at ^1H spectrometer frequencies of 500 and 800 MHz. This material is available free of charge via the Internet at http://pubs.acs.org.

REFERENCES

1. Stroppolo, M. E., Falconi, M., Caccuri, A. M., and Desideri, A. (2001) Superefficient enzymes. *Cell. Mol. Life Sci. 58*, 1451–1460.
2. Hammes, G. G. (2002) Multiple conformational changes in enzyme catalysis. *Biochemistry 41*, 8221–8228.
3. Schnell, J. R., Dyson, H. J., and Wright, P. E. (2004) Structure, dynamics and catalytic function of dihydrofolate reductase. *Annu. Rev. Biophys. Biomol. Struct. 33*, 119–140.
4. Hammes-Schiffer, S., and Benkovic, S. J. (2006) Relating protein motion to catalysis. *Annu. Rev. Biochem. 75*, 519.
5. Sawaya, M. R., and Kraut, J. (1997) Loop and subdomain movements in the mechanism of *Escherichia coli* dihydrofolate reductase: Crystallographic evidence. *Biochemistry 36*, 586–603.
6. Benkovic, S. J., Fierke, C. A., and Naylor, A. M. (1988) Insights into enzyme function from studies on mutants of dihydrofolate reductase. *Science 239*, 1105–1110.
7. Hammes-Schiffer, S. (2004) Quantum-classical simulation methods for hydrogen transfer in enzymes: A case study of dihydrofolate reductase. *Curr. Opin. Struct. Biol. 14*, 192–201.

8. Fierke, C. A., Johnson, K. A., and Benkovic, S. J. (1987) Construction and evaluation of the kinetic scheme associated with dihydrofolate reductase from *Escherichia coli*. *Biochemistry 26*, 4085–4092.
9. Venkitakrishnan, R. P., Zaborowski, E., McElheny, D., Benkovic, S. J., Dyson, H. J., and Wright, P. E. (2004) Conformational changes in the active site loops of dihydrofolate reductase during the catalytic cycle. *Biochemistry 43*, 16046–16055.
10. Adams, J., Johnson, K., Matthews, R., and Benkovic, S. J. (1989) Effects of distal point-site mutations on the binding and catalysis of dihydrofolate reductase from *Escherichia coli*. *Biochemistry 28*, 6611–6618.
11. Cameron, C. E., and Benkovic, S. J. (1997) Evidence for a functional role of the dynamics of glycine-121 of *Escherichia coli* dihydrofolate reductase obtained from kinetic analysis of a site-directed mutant. *Biochemistry 36*, 15792–15800.
12. Miller, G. P., and Benkovic, S. J. (1998) Strength of an interloop hydrogen bond determines the kinetic pathway in catalysis by *Escherichia coli* dihydrofolate reductase. *Biochemistry 37*, 6336–6342.
13. Miller, G. P., and Benkovic, S. J. (1998) Deletion of a highly motional residue affects formation of the Michaelis complex for *Escherichia coli* dihydrofolate reductase. *Biochemistry 37*, 6327–6335.
14. Miller, G. P., Wahnon, D. C., and Benkovic, S. J. (2001) Interloop contacts modulate ligand cycling during catalysis by *Escherichia coli* dihydrofolate reductase. *Biochemistry 40*, 867–875.
15. Rajagopalan, P. T., Lutz, S., and Benkovic, S. J. (2002) Coupling interactions of distal residues enhance dihydrofolate reductase catalysis: Mutational effects on hydride transfer rates. *Biochemistry 41*, 12618–12628.
16. Epstein, D. M., Benkovic, S. J., and Wright, P. E. (1995) Dynamics of the dihydrofolate reductase folate complex: Catalytic sites and regions known to undergo conformational change exhibit diverse dynamical features. *Biochemistry 34*, 11037–11048.
17. Falzone, C. J., Wright, P. E., and Benkovic, S. J. (1994) Dynamics of a flexible loop in dihydrofolate reductase from *Escherichia coli* and its implication for catalysis. *Biochemistry 33*, 439–442.
18. Osborne, M. J., Schnell, J., Benkovic, S. J., Dyson, H. J., and Wright, P. E. (2001) Backbone dynamics in dihydrofolate reductase complexes: Role of loop flexibility in the catalytic mechanism. *Biochemistry 40*, 9846–9859.
19. Schnell, J. R., Dyson, H. J., and Wright, P. E. (2004) Effect of cofactor binding and loop conformation on side chain methyl dynamics in dihydrofolate reductase. *Biochemistry 43*, 374–383.
20. McElheny, D., Schnell, J. R., Lansing, J. C., Dyson, H. J., and Wright, P. E. (2005) Defining the role of active-site loop fluctuations in dihydrofolate reductase catalysis. *Proc. Natl. Acad. Sci. U.S.A. 102*, 5032–5037.
21. Boehr, D. D., McElheny, D., Dyson, H. J., and Wright, P. E. (2006) The dynamic energy landscape of dihydrofolate reductase catalysis. *Science 313*, 1638–1642.
22. Loria, J. P., Rance, M., and Palmer, A. G. (1999) A relaxation-compensated Carr-Purcell-Meiboom-Gill sequence for characterizing chemical exchange by NMR spectroscopy. *J. Am. Chem. Soc. 121*, 2331–2332.
23. Palmer, A. G., Kroenke, C. D., and Loria, J. P. (2001) Nuclear magnetic resonance methods for quantifying microsecond-to-millisecond motions in biological macromolecules. *Methods Enzymol. 339*, 204–238.
24. Palmer, A. G. (2001) Nmr probes of molecular dynamics: Overview and comparison with other techniques. *Annu. Rev. Biophys. Biomol. Struct. 30*, 129–155.
25. Ferry, J. D., Grandine, L. D. J., and Fitzgerald, E. R. (1953) The relaxation distribution function of polyisobutylene in the transition from rubber-like to glass-like behavior. *J. Appl. Phys. 24*, 911–921.
26. Denisov, V. P., Peters, J., Hörlein, H. D., and Halle, B. (1996) Using buried water molecules to explore the energy landscape of proteins. *Nat. Struct. Biol. 3*, 505–509.
27. Ansari, A., Jones, C. M., Henry, E. R., Hofrichter, J., and Eaton, W. A. (1992) The role of solvent viscosity in the dynamics of protein conformational changes. *Science 256*, 1796–1798.
28. Qian, H. (2002) From discrete protein kinetics to continuous Brownian dynamics: A new perspective. *Protein Sci. 11*, 1–5.
29. Mulder, F. A., Mittermaier, A., Hon, B., Dahlquist, F. W., and Kay, L. E. (2001) Studying excited states of proteins by NMR spectroscopy. *Nat. Struct. Biol. 8*, 932–935.
30. Benkovic, S. J., and Hammes-Schiffer, S. (2003) A perspective on enzyme catalysis. *Science 301*, 1196–1202.
31. Beach, H., Cole, R., Gill, M. L., and Loria, J. P. (2005) Conservation of μs-ms enzyme motions in the apo- and substrate-mimicked state. *J. Am. Chem. Soc. 127*, 9167–9176.
32. Kovrigin, E. L., and Loria, J. P. (2006) Enzyme Dynamics along the Reaction Coordinate: Critical Role of a Conserved Residue. *Biochemistry 45*, 2636–2647.
33. Eisenmesser, E. Z., Millet, O., Labeikovsky, W., Korzhnev, D. M., Wolf-Watz, M., Bosco, D. A., Skalicky, J. J., Kay, L. E., and Kern, D. (2005) Intrinsic dynamics of an enzyme underlies catalysis. *Nature 438*, 117–121.
34. Wolf-Watz, M., Thai, V., Henzler-Wildman, K., Hadjipavlou, G., Eisenmesser, E. Z., and Kern, D. (2004) Linkage between dynamics and catalysis in a thermophilic-mesophilic enzyme pair. *Nat. Struct. Mol. Biol. 11*, 945–949.
35. Agarwal, P. K., Billeter, S. R., Rajagopalan, P. T. R., Benkovic, S. J., and Hammes-Schiffer, S. (2002) Network of coupled promoting motions in enzyme catalysis. *Proc. Natl. Acad. Sci. U.S.A. 99*, 2794–2799.
36. Watney, J. B., Agarwal, P. K., and Hammes-Schiffer, S. (2003) Effect of mutation on enzyme motion in dihydrofolate reductase. *J. Am. Chem. Soc. 125*, 3745–3750.
37. Wong, K. F., Selzer, T., Benkovic, S. J., and Hammes-Schiffer, S. (2005) Impact of distal mutations on the network of coupled motions correlated to hydride transfer in dihydrofolate reductase. *Proc. Natl. Acad. Sci. U.S.A. 102*, 6807–6812.
38. Sikorski, R. S., Wang, L., Markham, K. A., Rajagopalan, P. T., Benkovic, S. J., and Kohen, A. (2004) Tunneling and coupled motion in *Escherichia coli* dihydrofolate reductase catalysis. *J. Am. Chem. Soc. 126*, 4778–4779.
39. Wang, L., Goodey, N. M., Benkovic, S. J., and Kohen, A. (2006) Coordinated effects of distal mutations on environmentally coupled tunneling in dihydrofolate reductase. *Proc. Natl. Acad. Sci. U.S.A. 103*, 15753–15758.
40. Wang, L., Goodey, N. M., Benkovic, S. J., and Kohen, A. (2006) The role of enzyme dynamics and tunnelling in catalysing hydride transfer: Studies of distal mutants of dihydrofolate reductase. *Philos. Trans. R. Soc. London, Ser. B 361*, 1307–1315.
41. Rajagopalan, P. T., Zhang, Z., McCourt, L., Dwyer, M., Benkovic, S. J., and Hammes, G. G. (2002) Interaction of dihydrofolate reductase with methotrexate: Ensemble and single-molecule kinetics. *Proc. Natl. Acad. Sci. U.S.A. 99*, 13481–13486.
42. Zhang, Z., Rajagopalan, P. T., Selzer, T., Benkovic, S. J., and Hammes, G. G. (2004) Single-molecule and transient kinetics investigation of the interaction of dihydrofolate reductase with NADPH and dihydrofolate. *Proc. Natl. Acad. Sci. U.S.A. 101*, 2764–2769.
43. Antikainen, N. M., Smiley, R. D., Benkovic, S. J., and Hammes, G. G. (2005) Conformation coupled enzyme catalysis: Single-molecule and transient kinetics investigation of dihydrofolate reductase. *Biochemistry 44*, 16835–16843.
44. Kohen, A., Cannio, R., Bartolucci, S., and Klinman, J. P. (1999) Enzyme dynamics and hydrogen tunnelling in a thermophilic alcohol dehydrogenase. *Nature 399*, 496–499.
45. Liang, Z. X., Lee, T., Resing, K. A., Ahn, N. G., and Klinman, J. P. (2004) Thermal-activated protein mobility and its correlation with catalysis in thermophilic alcohol dehydrogenase. *Proc. Natl. Acad. Sci. U.S.A. 101*, 9556–9561.
46. Knapp, M. J., Rickert, K., and Klinman, J. P. (2002) Temperature-dependent isotope effects in soybean lipoxygenase-1: Correlating hydrogen tunneling with protein dynamics. *J. Am. Chem. Soc. 124*, 3865–3874.
47. Kovrigin, E. L., and Loria, J. P. (2006) Characterization of the Transition State of Functional Enzyme Dynamics. *J. Am. Chem. Soc. 128*, 7724–7725.
48. Watt, E. D., Shimada, H., Kovrigin, E. L., and Loria, J. P. (2007) The mechanism of rate-limiting motions in enzyme function. *Proc. Natl. Acad. Sci. U.S.A. 104*, 11981–11986.
49. Swint-Kruse, L., and Fisher, H. F. (2008) Enzymatic reaction sequences as coupled multiple traces on a multidimensional landscape. *Trends Biochem. Sci. 33*, 104–112.
50. Benkovic, S. J., Hammes, G. G., and Hammes-Schiffer, S. (2008) Free-Energy Landscape of Enzyme Catalysis. *Biochemistry 47*, 3317–3321.
51. Skrynnikov, N. R., Dahlquist, F. W., and Kay, L. E. (2002) Reconstructing NMR spectra of "invisible" excited protein states using HSQC and HMQC experiments. *J. Am. Chem. Soc. 124*, 12352–12360.

BI801102E